SHIP WAKE DETECTION IN X-BAND SAR IMAGES USING SPARSE GMC REGULARIZATION

Oktay Karakuş, Alin Achim

Visual Information Lab, University of Bristol, Bristol, U.K.

ABSTRACT

Ship wakes have crucial importance in the analysis of SAR images of the sea surface due to the information they carry about vessels. Since ship wakes mostly appear as lines in SAR images, line detection methods have been widely used for their identification. In the literature, common practice for detecting ship wakes is to use Hough and Radon transforms in which bright (dark) lines appear as peaks (troughs) points. In this paper, the ship wake detection problem is addressed as a Radon transform based inverse problem with a sparse non-convex *generalized minimax concave* (GMC) regularization. Despite being a non-convex regularizer, the GMC penalty enforces the cost function to be convex. The solution to this convex cost function optimisation is obtained in a Bayesian formulation and the lines are recovered as *maximum a posteriori* (MAP) point estimates with a sparse GMC based prior. The detection procedure consists of a restricted area search in the Radon domain and the validation of candidate wakes. The performance of the proposed method is demonstrated in TerraSAR-X images of five different ships and with a total of 19 visible ship wakes. The results show a successful detection performance of up to 84% for the utilised images.

Index Terms— Ship Wake Detection, MAP Estimation, Inverse Problem, GMC Regularization

1. INTRODUCTION

Synthetic aperture radar (SAR) images of moving ships exhibit characteristic patterns determined by different wake formation processes which are typically considered to fall in one of three categories: (i) surface waves created by ships, (ii) turbulent wakes, and (iii) ship-generated internal waves [1]. Ship-generated surface waves are commonly described as a composite model. Under this framework, one component of the model includes the short (centimeter scale) waves, which are observed in SAR images through the Bragg scattering mechanism [2], and appear as bright, narrow V wakes. The second subcategory includes the (decameter scale) waves forming the classical Kelvin wake system [3]. This two-scale composite model has been used in [4] to simulate the intensity of SAR images of a rough sea surface with an embedded Kelvin wake. Fujimura et al. [5] assessed the validity of a simulated ship wake using methods of computational dynamics, using real TerraSAR-X data.

Since ship wakes are linear structures, detection methods are mostly based on line feature detection approaches, such as Hough or Radon transforms, both of which create bright peaks in the transform domain for bright lines in images, and troughs for dark lines. Due to its high computational cost, Hough transform is less popular than the Radon transform [6]. Radon transform is widespread in ship wake detection applications with its lower computational requirements. Despite its popularity, Radon transform has a couple of drawbacks, e.g. bright pixels belonging to ships potentially causing false detections [7]. Hence, enhancing the information in Radon domain is commonly used in practice to cope with its disadvantages [4, 8, 9, 10]. A wake detection method has been proposed by Graziano et. al. [6, 11] and deals directly with the noisy image without any enhancement. Moreover, in [6, 11], Radon transform of the ship-centred and masked image tile has first been restricted and then been searched to detect peaks (trough) points.

Inverse problem formulation for generic line detection applications has first been proposed by Aggarwal and Karl [12]. The main advantage of formulating line detection as an inverse problem is that it allows the incorporation of prior information about the object of interest. Anantrasirichai et al. [13] have also exploited this for B-line detection in lung ultrasound images.

In this paper, we propose a novel inverse problem based approach to ship wake detection in SAR images. The solution to this inverse problem uses a Bayesian formulation, which leads to a *maximum a-posteriori* (MAP) estimator. Our proposed formulation incorporates the generalized minimax concave (GMC) penalty of Selesnick [14] as regularization term. Using GMC penalty demonstrates the advantages of using non-convex sparse penalties while enforcing the cost function to remain convex, i.e. having a log-concave posterior. We utilize TerraSAR-X images to test the performance of the proposed method. For the detection step, we follow the method in [6, 11] which uses real ancillary data, local map, ship clusters, local traffic statistics to determine some of the parameters during the pre-processing step. Our proposed method detects ship wakes independently from the real information about the ships and the environment by roughly selecting the required parameters. MAP estimates are obtained by using the forward-backward (FB) algorithm.

The rest of the paper is organized as follows: the inverse problem formulation is discussed in Section 2. In Section 3, MAP estimation with a GMC prior is presented. SAR datasets and the detection algorithm are described in Sections 4 and 5, respectively. Experimental studies and results are provided in Section 6 and Section 7 concludes the paper with a summary and remarks.

2. SHIP WAKES AND IMAGE FORMATION MODEL

Typically, a moving ship in deep-sea creates different types of wakes (i.e. linear structures in SAR images). Of these, the central dark streak is named as *turbulent wake*. A turbulent wake is often bounded with two bright wakes which are called *Narrow-V wakes*, the half-angle of which lies between 1.5° and 4° [6, 10]. The outer wakes which limit the moving ship signatures on the sea surface are *Kelvin wakes* which are located at both sides of the turbulent wake with a limiting half angle of 19.5°. In SAR images, Kelvin wakes can be somewhat narrower and lie within half-angles of 10° and

This work was supported by the Engineering and Physical Sciences Research Council (EPSRC) under grant EP/R009260/1 (AssenSAR).

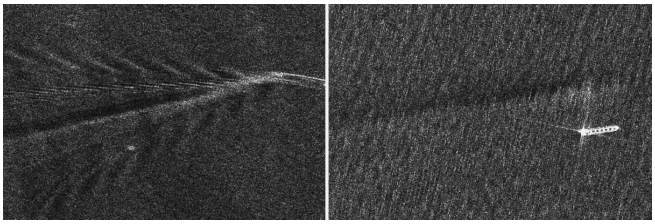

Fig. 1. Example SAR images. (Left) - Image with 5 ship wakes. (Right) - Image without Kelvin wakes.

19.5° [4]. An example SAR image including all five ship wakes is depicted in Figure 1-(left). However, in most of the SAR images of moving ships, all these wakes are rarely visible. Generally, one of the narrow-V and/or Kelvin wakes can not be observed. In Figure 1-(right), an example SAR image of a moving ship without Kelvin wakes is depicted.

A SAR image formation model using ship wakes modelled as lines in the Radon domain can be expressed as

$$Y = \mathcal{C}X + N, \tag{1}$$

where Y is the $M \times M$ observed noisy SAR image and $X(r, \theta)$ is the image in Radon domain representing lines by a distance r from the centre of image Y and an orientation θ from the horizontal axis of the image. In addition, N is additive noise, which is generally assumed to be Gaussian and the operator $\mathcal{C}$ represents the inverse Radon transform $\mathcal{R}^{-1}$.

In image analysis, the Radon transform $x(r, \theta)$ of an image $y(i, j)$ ($x = \mathcal{R}y$) is a line integral of the image intensities, given in (2), over the hyperplane perpendicular to θ.

$$x(r, \theta) = \int_{\mathbb{R}^2} y(i, j)\delta(r - i\cos\theta - j\sin\theta)didj \tag{2}$$

where $\delta(\cdot)$ is the Dirac-delta function. Here we use discrete operators $\mathcal{R}$ and $\mathcal{C}$ as in [15].

3. MAP ESTIMATION

3.1. Bayesian Inference

Assume we need to estimate the object of interest (unknown) signal x and we are given the observation signal y related to x. In addition, the observation signal has a statistical model, which defines its relation to x and is referred to as the likelihood $p(y|x)$. Obtaining x from y might be very problematic and ill-posed, thus the estimate can have lots of uncertainties. Using Bayesian inference methods helps to reduce this uncertainty by utilising prior knowledge on the unknown signal x. The prior $p(x)$ can promote structural properties such as sparsity.

Hence, combining this prior with the observed statistical model creates the posterior distribution via Bayes' theorem as

$$p(x|y) = \frac{p(y|x)p(x)}{\int p(y|x)p(x)dx} \tag{3}$$

where $p(x|y)$ models the knowledge on x given the knowledge on y. The denominator $\int p(y|x)p(x)dx$ in (3) is the marginal likelihood of y (i.e. $p(y)$) which is not related to x and is constant. Hence, we can easily write the unnormalized posterior distribution as

$$p(x|y) \propto p(y|x)p(x). \tag{4}$$

In most cases, the posterior distributions are log-concave (which is not strictly to be). Hence they can be represented as

$$p(x|y) \propto \exp\{-F_y(x)\} \tag{5}$$

where $F_y(x)$ is a convex function. In order to obtain a point estimate $\hat{x}$, maximum a-posteriori (MAP) estimators can be used as

$$\hat{x}_{\text{MAP}} = \arg\max_x p(x|y) = \arg\min_x F_y(x). \tag{6}$$

When $F_y(x)$ is not convex, the minimizer will not be convex but nevertheless can be solved via proximal operators [16]. If a point estimate is not enough, more complex Bayesian approaches can be used. Proximal Markov chain Monte Carlo (p-MCMC) methods [17, 18, 19] are important example approaches for problems of this type. Despite MAP being a point estimator, it serves the purpose of this study and p-MCMC methods are out of the scope of this paper.

3.2. Sparse MAP Estimation for Ship Wakes

In a standard normal i.i.d. noise case, the likelihood distribution of the observed noisy SAR image Y with respect to the desired line image X, is

$$p(Y|X) \propto \exp\{-\|Y - \mathcal{C}X\|_2^2\}. \tag{7}$$

Assume we have priors in the form of $p(X) \propto \exp\{-\lambda\psi(X)\}$. Then, from Bayes' theorem, the cost function $F_Y(X)$ can be written as

$$F_Y(X) \propto \|Y - \mathcal{C}X\|_2^2 + \lambda\psi(X), \tag{8}$$

where λ is the scale parameter of the prior distribution, or the regularization constant. As long as the cost function $F_Y(X)$ is convex, solving and obtaining point estimates is easier than in the non-convex case. On the other hand, it is clear that non-convex penalties can sometimes handle sparse problems better than the convex ones. The GMC penalty has been proposed by Selesnick [14] as a sparsity enforcing non-convex regularization term, which demonstrates the advantages of using non-convex penalties by preserving the convexity of the cost function at the same time. It is based on L_1 norm and the generalized Huber function. In [14] it has been shown that the GMC penalty outperforms the other common penalties in noise removal applications.

The GMC penalty function can be defined as [14]

$$\psi_B(t) = \|t\|_1 - S_B(t) \tag{9}$$

where $S_B(t) = \inf_v\{\|v\|_1 + \frac{1}{2}\|B(t - v)\|_2^2\}$ is the generalized huber function. The scaling matrix B should be selected in relation to $\mathcal{C}$ to provide convexity of the cost function $F_Y(X)$ as $B = \sqrt{\frac{\gamma}{\lambda}}\mathcal{C}$ where γ is a parameter which controls the degree of non-convexity of the penalty. Note that for $0 \leq \gamma \leq 1$, B will provide convexity of the cost function. The nominal range of $0.5 \leq \gamma \leq 0.9$ can be used for better performance [14].

In this study, we propose to use the GMC penalty in (9) as the prior on X

$$p(X) \propto \exp\{-\lambda\psi_B(X)\} \tag{10}$$

$$\propto \exp\{-\lambda\left(\|X\|_1 - S_B(X)\right)\}. \tag{11}$$

which leads to a MAP estimator with GMC prior

$$\hat{X}_{\text{MAP-GMC}} = \arg\min_{X} \max_{v} \Big\{ \|Y - \mathcal{C}X\|_2^2 + \lambda\|X\|_1 - \lambda\|v\|_1 - \gamma\|\mathcal{C}(X - v)\|_2^2 \Big\}. \quad (12)$$

The solution to this problem can be obtained using the FB algorithm (For details please see [14]). FB algorithm for GMC regularized cost functions requires only a couple of simple computational steps and soft-thresholding, which is the proximal operator for L_1 based regularization. The FB pseudo-code to solve (12) is given in Algorithm 1 where $\mathcal{C}^T$ refers to the inverse of $\mathcal{C}$, namely the Radon transform $\mathcal{R}$. For the purpose of this study, we have selected the maximum number of iterations $MaxIter = 1000$ and the stopping criteria as 10^{-3}, which can be calculated for iteration i as $\epsilon^{(i)} = \|X^{(i)} - X^{(i-1)}\|/\|X^{(i-1)}\|$.

Algorithm 1 Forward-backward (FB) algorithm for GMC regularized cost function

Inputs: Ship-centered image Y, $\lambda > 0$, $0.5 \leq \gamma \leq 0.9$
Output: Radon image X
Set: $0 < \mu < 1.9$ and $i = 0$
do
  $w^{(i)} = X^{(i)} - \mu\mathcal{C}^T(\mathcal{C}(X^{(i)} + \gamma(v^{(i)} - X^{(i)})) - Y)$
  $u^{(i)} = v^{(i)} - \mu\gamma\mathcal{C}^T\mathcal{C}(v^{(i)} - X^{(i)})$
  $X^{(i)} = soft(w^{(i)}, \mu\lambda)$
  $v^{(i)} = soft(u^{(i)}, \mu\lambda)$
  $i++$
while $\epsilon^{(i)} > 10^{-3}$ or $i < MaxIter$

Table 1. Visible wakes in used SAR images.

Image	Turbulent	1st Narrov	2nd Narrov	1st Kelvin	2nd Kelvin
TX1-Gib1	✓	✓	✓	✓	✓
TX2-Gib2	✓	✓	✗	✓	✗
TX3-Sin1	✓	✓	✗	✓	✓
TX4-Sin3	✓	✓	✗	✓	✗
TX5-USA	✓	✓	✗	✓	✓

4. SAR DATA SETS

In order to test the performance of the proposed approach, we have used 3 different TerraSAR-X images[1] from Gibraltar, Singapore and the USA, all of which are Stripmap products with three meters resolution for both azimuth and range directions. Singapore and Gibraltar images are in HH polarization where USA is in VV polarization. In these images, five different ship wake patterns have been selected (i.e. 5 different ships with some visible wakes) by visual inspection. Then, ship centred image tiles are created as the input of the detection procedure. We assume that ship locations for the selected ships are known. This step can be replaced in practice with ship detection techniques such as constant false alarm rate (CFAR) approach in Pappas et al. [20].

All the ships in the created ship centred image tiles are subsequently masked, to remove bright points in Radon domain arising from the ship itself. Masking is performed by firstly selecting a rectangle area including the ship which is then replaced with the mean intensity of the image. Masking the ships ensures the interpretation of bright points as possible ship wakes in Radon domain.

[1]The TerraSAR-X images are sample products which are provided by Airbus Defence and Space in http://www.intelligence-airbusds.com/en/8262-sample-imagery

In Table 1, each image tile is given with the type of visible ship wakes identified by visual inspection. It is clear that only one tile (TX1-Gib1) has all possible wakes whereas the rest have less than five. Overall, we have 19 detectable (visible) out of 25 (all possible wakes for 5 ships) ship wakes in all images. The performance evaluation has been performed in terms of true detections of these ship wakes.

5. SHIP WAKE DETECTION

The detection algorithm in this paper, includes three important steps: 1) Pre-processing and inverse problem solution, 2) detection of wakes in the Radon domain and 3) validation in the image domain.

The pre-processing step includes creating ship-centred-masked image tiles and inverse problem solution. Image centring and masking operations in this paper have been discussed in the previous section. Note that in Graziano et. al. [6] the masking operation step is slightly different from the one in this paper. In their detection method, instead of replacing the ship area with the mean intensity, only the unmasked pixels have been taken into account (for details please see p.4 in [6]).

Following the pre-processing step, the peak/trough searching area in the Radon domain (r, θ) is restricted. We ensure that peaks/trough belong to all possible wakes should lie between two sine waves [9, 6] with: $|r| \leq A \sin\theta$. The peak points of sine waves A is normally the maximum azimuth shift and can be calculated from the real measurements of the area such as slant range, antenna velocity and ship velocity along the slant range. Due to not having real ship information for the images, we roughly select A depending on the number of pixels in image azimuth dimension M.

The next step is detecting a peak/trough pair which corresponding to turbulent and first-narrow-V wake pair (T-N pair). A window size of 4° is scanned and the pair which maximizes the difference in amplitudes is selected as the T-N pair. Then, the second narrow-V wake is detected by searching the other side of the detected turbulent wake where the first narrow-V wake is not located. The maximum point within a 4° of the window is selected as the second narrow-V wake. In order to detect Kelvin wakes, both sides of the detected turbulent wake are searched. The window size for Kelvin wakes is from 10° to 20° which follows the physical characteristics of the Kelvin wakes.

After detecting candidate points for all five wakes, the following step is the validation, which is performed in the image domain. In order to obtain five different lines in the image domain, the inverse Radon transform is firstly applied to detected points in the previous steps. All five lines (or fewer) cover the whole image. Thus, half of the lines should be removed (which is called the 180° ambiguity problem [6]). To solve this ambiguity, only the detected turbulent wake is used. The average intensity over the line representing the detected turbulent wake is calculated and the half line having a lower average (as turbulent wake is a dark line) is selected as the un-confirmed half line. Half lines belonging to the other detected wakes are selected as the ones which are located $\pm 45^\circ$ around the un-confirmed turbulent wake half line.

The last step of the detection process is the confirmation for the candidate half lines. Hence, a measure index F is used and can be calculated as: $F = \bar{I}_w/\bar{I} - 1$ [21]. This index is a measure that compares the average intensity over the un-confirmed wake, $\bar{I}_w$, to the average intensity of the image, $\bar{I}$. The F index value should be positive for bright wakes and negative only for the turbulent wake.

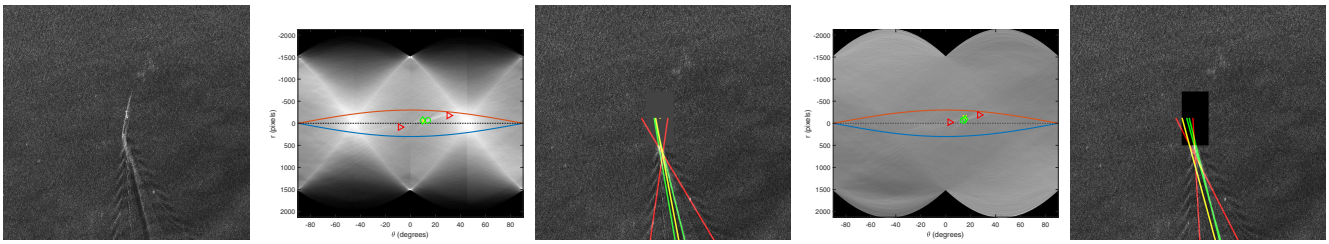

(a) (b) (c) (d) (e)

Fig. 2. Ship wake detection results for TX1-Gib1 image tile. (a) Ship centred image tile (unmasked), (b) Detected points in radon domain for the proposed method. (c) Detected lines - the proposed method, (d) Detected points in radon domain for the Graziano et. al. [6], (e) Detected lines - Graziano et. al. [6]. Yellow points (lines) refer to turbulent wake when green and red points (lines) represent narrow-V and Kelvin wakes, respectively. Grey and black rectangles in (c) and (e) are masked areas.

Detected half lines that do not follow this rule are discarded, whereas the remaining half lines are confirmed.

6. EXPERIMENTAL RESULTS

The performance of the proposed method has been demonstrated for five ship-centred-marked image tiles. In particular, the aim is to detect 19 possible ship wakes and to discard 6 invisible wakes. The proposed method parameters are selected as $\lambda = 50$ and $\gamma = 0.9$ by trial-and-error. The range for angle θ for all the data sets and methods is defined as $-90 \leq \theta \leq 90$. For computational ease, the angle range is divided into four intervals of 45 degrees and for each subrange, the MAP estimator is performed. Then, all obtained results are combined to obtain a complete radon image, $\hat{X}_{\text{MAP-GMC}}$.

In Table 2, the detection performance of the methods is quantified. A range between $L/5$ and $L/15$ for A has been searched first and the best results are depicted in the table. Both the proposed method and Graziano et. al. achieved the best detection performance for $A = L/10$. Percentages in Table 2 show true and false detections. True confirmation refers to the confirmed detection of visible wakes in the image and true discard represents confirmed discard of invisible wakes. False confirmation is the confirmed detection of invisible wakes. Detection of a visible wake in a wrong location is handled as a false detection. Examining the values in Table 2, the proposed method correctly detects the ship wakes in 84% of the cases whereas Graziano et. al. achieves 64%. Even though their performance has been up to 80% in their papers [6, 11, 7, 21], for the data sets and the parameter setting in this paper, their performance is lower.

In Figure 2, the detection performance can be visually assessed both in the image domain and the Radon domain. For TX1-Gib1 image tile, all five ship wakes are visible and both methods detected five ship wakes. Graziano et. al. detected one of the narrow-V wakes in a wrong location. Even though detected Kelvin wakes do appear different for both methods in Figure 2-(c) and 2-(e), detected Kelvin wakes are in the theoretical angle range with respect to the detected turbulent wake for both methods.

Table 2. Detection performance over all data sets ($A = L/10$).

	True Detection		False Detection	
	Confirmation	Discards	Confirmation	Wrong Location
Proposed Method	72%	12%	12%	4%
Graziano et. al. [6]	64%	0%	24%	12%

7. CONCLUSIONS

We proposed an inverse problem formulation for ship wake detection in SAR images based on a GMC penalty. The problem was addressed in a Bayesian framework and the objects of interest are recovered via MAP estimation. Due to GMC penalty's ability to preserve the convexity of the cost function, the MAP point estimates can be calculated via convex optimization. After the enhanced Radon image is obtained, a powerful ship detection method is employed, similar to [6, 11]. The performance was evaluated for different TerraSAR-X images and the proposed method is shown to achieve a true detection performance of 84%.

We conclude that an enhancement in Radon space increases the detectability of the peaks/through compared to the direct approach in Graziano et. al. and makes the proposed method detect ship wakes more accurately. This is especially true when input SAR images are particularly noisy.

Future work will combine the proposed method with autofocusing in SAR images. Investigating more complex sparsity enforcing priors in conjunction with non-convex optimization algorithms is also one of our current endeavors.

8. REFERENCES

[1] JW Wright, "A new model for sea clutter," *IEEE Transactions on antennas and propagation*, vol. 16, no. 2, pp. 217–223, 1968.

[2] Junjun Yin, Jian Yang, Zheng-Shu Zhou, and Jianshe Song, "The extended Bragg scattering model-based method for ship and oil-spill observation using compact polarimetric SAR," *IEEE Journal of Selected Topics in Applied Earth Observations and Remote Sensing*, vol. 8, no. 8, pp. 3760–3772, 2015.

[3] JW Wright and WC Keller, "Microwave-scattering and straining of wind-generated waves," in *Transactions-American Geophysical Union*. American Geophysical Union 2000 Florida Ave NW, Washington, DC 20009, 1974, vol. 55, pp. 1137–1137.

[4] Gregory Zilman, Anatoli Zapolski, and Moshe Marom, "On detectability of a ship's Kelvin wake in simulated SAR images of rough sea surface," *IEEE Transactions on Geoscience and Remote Sensing*, vol. 53, no. 2, pp. 609–619, 2015.

[5] Atsushi Fujimura, Alexander Soloviev, and Vladimir Kudryavtsev, "Numerical simulation of the wind-stress

effect on SAR imagery of far wakes of ships," *IEEE Geoscience and Remote Sensing Letters*, vol. 7, no. 4, pp. 646–649, 2010.

[6] Maria Daniela Graziano, Marco D'Errico, and Giancarlo Rufino, "Wake component detection in X-band SAR images for ship heading and velocity estimation," *Remote Sensing*, vol. 8, no. 6, pp. 498, 2016.

[7] Maria Daniela Graziano, Marco D'Errico, and Giancarlo Rufino, "Ship heading and velocity analysis by wake detection in SAR images," *Acta Astronautica*, vol. 128, pp. 72–82, 2016.

[8] M. T. Rey, J. K. Tunaley, J. T. Folinsbee, P. A. Jahans, J. A. Dixon, and M. R. Vant, "Application Of Radon Transform Techniques To Wake Detection In Seasat-A SAR Images," *IEEE Transactions on Geoscience and Remote Sensing*, vol. 28, no. 4, pp. 553–560, July 1990.

[9] James KE Tunaley, "The estimation of ship velocity from SAR imagery," in *Geoscience and Remote Sensing Symposium, 2003. IGARSS'03. Proceedings. 2003 IEEE International*. IEEE, 2003, vol. 1, pp. 191–193.

[10] Gregory Zilman, Anatoli Zapolski, and Moshe Marom, "The speed and beam of a ship from its wake's SAR images," *IEEE Transactions on Geoscience and Remote Sensing*, vol. 42, no. 10, pp. 2335–2343, 2004.

[11] Maria Daniela Graziano, Marco Grasso, and Marco D'Errico, "Performance Analysis of Ship Wake Detection on Sentinel-1 SAR Images," *Remote Sensing*, vol. 9, no. 11, pp. 1107, 2017.

[12] Nitin Aggarwal and W Clem Karl, "Line detection in images through regularized Hough transform," *IEEE transactions on image processing*, vol. 15, no. 3, pp. 582–591, 2006.

[13] Nantheera Anantrasirichai, Wesley Hayes, Marco Allinovi, David Bull, and Alin Achim, "Line detection as an inverse problem: application to lung ultrasound imaging," *IEEE transactions on medical imaging*, vol. 36, no. 10, pp. 2045–2056, 2017.

[14] Ivan Selesnick, "Sparse regularization via convex analysis," *IEEE Transactions on Signal Processing*, vol. 65, no. 17, pp. 4481–4494, 2017.

[15] Brian T Kelley and Vijay K Madisetti, "The fast discrete Radon transform. I. Theory," *IEEE Transactions on Image Processing*, vol. 2, no. 3, pp. 382–400, 1993.

[16] Peter J Green, Krzysztof Latuszyński, Marcelo Pereyra, and Christian P Robert, "Bayesian computation: a summary of the current state, and samples backwards and forwards," *Statistics and Computing*, vol. 25, no. 4, pp. 835–862, 2015.

[17] Marcelo Pereyra, "Proximal Markov chain Monte Carlo algorithms," *Statistics and Computing*, vol. 26, no. 4, pp. 745–760, 2016.

[18] Xiaohao Cai, Marcelo Pereyra, and Jason D McEwen, "Uncertainty quantification for radio interferometric imaging–I. Proximal MCMC methods," *Monthly Notices of the Royal Astronomical Society*, vol. 480, no. 3, pp. 4154–4169, 2018.

[19] Alain Durmus, Eric Moulines, and Marcelo Pereyra, "Efficient Bayesian computation by proximal Markov chain Monte Carlo: when Langevin meets Moreau," *SIAM Journal on Imaging Sciences*, vol. 11, no. 1, pp. 473–506, 2018.

[20] Odysseas Pappas, Alin Achim, and David Bull, "Superpixel-Level CFAR Detectors for Ship Detection in SAR Imagery," *IEEE Geoscience and Remote Sensing Letters*, vol. 15, no. 9, pp. 1397–1401, 2018.

[21] M Daniela Graziano, Giancarlo Rufino, and Marco D'Errico, "Wake-based ship route estimation in high-resolution SAR images," in *SAR Image Analysis, Modeling, and Techniques XIV*. International Society for Optics and Photonics, 2014, vol. 9243, p. 92430T.